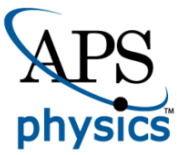

Exchange-Coupling-Induced Symmetry Breaking in Topological Insulators

Peng Wei, Ferhat Katmis, Badih A. Assaf, Hadar Steinberg, Pablo Jarillo-Herrero, Donald Heiman, and Jagadeesh S. Moodera

Phys. Rev. Lett. **110**, 186807 — Published 30 April 2013

DOI: 10.1103/PhysRevLett.110.186807

Exchange coupling induced symmetry breaking in topological insulators

Peng Wei[1*], Ferhat Katmis[1,2], Badih A. Assaf[3], Hadar Steinberg[2], Pablo Jarillo-Herrero[2], Donald Heiman[3] and Jagadeesh S. Moodera[1,2*]

[1]*Francis Bitter Magnet Laboratory,* [2]*Department of Physics, Massachusetts Institute of Technology, Cambridge, Massachusetts 02139, USA*
[3]*Department of Physics, Northeastern University, Boston, Massachusetts 02115, USA*

An exchange gap in the Dirac surface states of a topological insulator (TI) is necessary for observing the predicted unique features such as the topological magnetoelectric effect as well as to confine Majorana fermions. We experimentally demonstrate proximity-induced ferromagnetism in a TI, combining a ferromagnetic insulator EuS layer with Bi_2Se_3, without introducing defects. By magnetic and magnetotransport studies, including anomalous Hall effect and magnetoresistance measurements, we show the emergence of a ferromagnetic phase in TI, a step forward in unveiling their exotic properties.

(Dated: December 16, 2012)

*e-mail: pwei@mit.edu; moodera@MIT.EDU

Three-dimensional topological insulators (TIs) are materials carrying surface states protected by time reversal symmetry.[1,2] The short-range nature of magnetic proximity coupling with a ferromagnetic insulator (FI) allows the TI surface states to experience the ferromagnetic interactions, where the symmetry breaking happens right at the interface,[3-6] rather than affecting the majority bulk states or introducing defects. The well behaved Heisenberg FI such as EuS, is an excellent candidate to isolate the magnetic response of the surface states from the parallel conduction of the TI bulk material. Furthermore, the local time-reversal symmetry breaking is essential for inducing a quantized topological magnetoelectric response.[7] This may be used to investigate interesting emergent phenomena, such as the zero-field half-integer quantum Hall effect,[7] the topological magnetoelectric effect,[7,8] and the magnetic monopole,[9] to name a few.

Experimentally the most common method of introducing ferromagnetic order in TI is by doping with specific elements; in this case, it is hard to separate the surface and the bulk phases.[10-14] Although a surface ferromagnetic order is shown achievable by uniformly depositing magnetic atoms, *i.e*. Fe, over the TI surface,[15,16] the transport properties of a TI can be influenced by the metallic ferromagnetic overlayer/atoms. Besides, the doping of magnetic elements inevitably introduces crystal defects, magnetic scattering centers, as well as impurity states in the insulating gap, which are detrimental to mobility and the transport of spin-momentum locked surface electrons in TIs.[1] From the point of view of confining Majorana fermions in topological superconductors,[17,18] the exchange field of an FI is capable of lifting the spin degeneracy without destroying the superconductivity pairing.[5,6] This is in contrast to the adverse effects resulting from the introduction of magnetic impurities. In combination with an FI, the Majorana bound states can be well established on the top surface of a superconducting TI[19] or superconducting proximity-coupled TI.[20]

Here, we introduce ferromagnetic order onto the surface of Bi_2Se_3 thin films by using the FI EuS (Fig. 1a) forming Bi_2Se_3/EuS heterostructures. Ultra-thin FI EuS layers are stable with good growth characteristics and clean interface on a variety of materials; they form excellent tunnel barriers even down to 1 nm thickness showing near ideal area coverage.[5,6,21,22] Although the magnetic proximity effect of EuS on superconductor has been clearly demonstrated,[5] its effectiveness on the TI Dirac surface state is an open question. This exchange phenomenon can be expected to have profound influence on the novel surface

Dirac electron system, especially the spin-momentum locked helical electronic states in TIs.[1,23,24] Achieving this is nontrivial as it critically depends on the control of the TI/EuS heterostructures interface down to the last atomic layer to be able to transmit the exchange interaction across. This also depends on the growth condition of EuS on bismuth compounds.

The bilayer structure growth was carried out in a molecular beam epitaxy (MBE) apparatus in an ultra-high vacuum (UHV) environment (low 10^{-10} torr). Thin film Bi_2Se_3 were epitaxially grown on Si(111) or Al_2O_3(0001) substrates by coevaporating high-purity Bi and Se constituents from separate conventional Knudsen cells at 450 K. EuS was grown *in situ* on Bi_2Se_3 from a single e-beam source at room temperature, followed by a capping layer of 4 nm amorphous Al_2O_3 layer. The quality of the layers were confirmed by high-resolution X-ray diffraction (XRD), using 1.54 Å Cu-$K_{\alpha 1}$ radiation, which was also used to confirm the thickness and smoothness of the grown layers. Figure 1b shows the X-ray diffraction characterizations revealing the single phase of hexagonal Bi_2Se_3 and cubic EuS indicating the epitaxial growth without any clustering. The growth relations on sapphire and silicon substrates are Al_2O_3[0001]//Bi_2Se_3[0001]//EuS[111] and Si[111]//Bi_2Se_3[0001]//EuS[111]. Low angle x-ray reflectivity studies confirmed sharp Bi_2Se_3/EuS interface.

Several samples were grown simultaneously with a shadow mask technique. The Bi_2Se_3 layer thickness was fixed at 20 nm, while the EuS film thickness was varied locally (1, 3, 5, 7 and 10 nm in different lateral sections of the same Bi_2Se_3 film). Besides, a sample of 1 nm EuS on Si(111) was also grown *in situ* forming a set of TI/FI bilayer samples and single layer control sample for the studies. For transport measurements, control samples of Bi_2Se_3 thin films capped with Al_2O_3 were grown simultaneously. While the control samples did not display magnetic behavior, they showed typical weak anti-localization (WAL) effect under a perpendicular magnetic field (only a weak field dependence, and no WAL, for in-plane magnetic field) and with no hysteresis, as seen by others[25,26] as well as our previous observations.[27] The samples were patterned into standard Hall bar devices with a channel width of 60 μm and channel length of 400 μm. The charge carriers of the Bi_2Se_3 layers were determined to be n-type with a density (n_{3D}) ~ 4×10^{19} cm^{-3} at 4.2 K, which was not sensitive to the EuS capping. For several samples (both control and bilayer samples), temperature dependence of n_{3D} was monitored. We found only a small decrease (< 1%) in n_{3D} as the temperature went below ~ 40 K, with most decrease occurring below ~ 10 K in both bilayer and control samples. No significant change was observed for n_{3D} across T_C in bilayer samples due to the development of interface ferromagnetism. The large background contribution from the bulk conductivity could have precluded observing any changes across T_C.

The magnetic properties of the Bi_2Se_3/EuS heterostructures were determined by magnetization measurements, performed in a Quantum Design MPMS system. All TI/FI bilayer samples exhibit ferromagnetic phase transitions when the temperature decreases below about 20 K (Fig. 2a inset). Also shown here is the magnetic hysteresis loop with a sizeable remnant magnetization and coercive field H_c indicating an in-plane easy axis. The T_C was estimated from the point at which the slope of M vs T data sharply increased. It may be noted that the T_C is influenced by the applied field during cooling (unless this field is very small) as well as due to high carrier density. These factors can raise T_C above the bulk T_C of EuS.[28]

In the following we demonstrate that EuS induces a significant magnetic moment on the surface of the Bi_2Se_3 film. Figure 2a shows the measured magnetic moment of three bilayer samples having varying thicknesses, and a control sample of Si(111)/EuS. It is striking that for all Bi_2Se_3/EuS samples, *each Eu^{2+} ion contributes a saturation magnetic moment $M_{I,S}$ that is higher than the 7 μ_B upper limit of EuS*.[6] Moreover, $M_{I,S}$ increases as the thickness of the EuS layer decreases (inset of Fig. 2b). It reaches a maximum of 11.3 μ_B/Eu^{2+} in the bilayer sample with 1 nm EuS, which is 60% larger than the 7 μ_B/Eu^{2+} value.[6] It may be noted that the maximum number of deposited EuS molecules was monitored by the quartz sensor. Since the excess moment cannot be accounted for by the EuS layer alone, its origin is attributed to the induced moment at the Bi_2Se_3/EuS interface. On the other hand, the control sample shows a $M_{I,S}$ of 5.9 μ_B/Eu^{2+} (Fig. 2a), indicating that the enhanced moment seen in the Bi_2Se_3/EuS bilayer is not due to the EuS layer or the film thickness-related properties. Furthermore, EuS shows more favorable growth on Bi_2Se_3 compared to Si(111). The H_c of

1nm EuS on Bi_2Se_3 (~18 Oe) is three times larger than the H_c of 1nm EuS on Si(111), which is only 6 Oe.

The magnitude of the induced magnetization can be extracted through the following analysis. The total saturation moment is expressed as $M_s = 2J_z\mu_B\rho_N dA + m_0 A$. Here, the theoretical maximum is $J_z = 7/2$ for each Eu^{2+} ion in EuS,[6] d is the thickness of EuS film, A the area of the sample, and ρ_N the number density of Eu^{2+} ions. The induced magnetic moment at the interface is represented by m_0. A plot of M_s/A vs. d for five bilayer samples (Fig. 2b) shows linear dependence. A linear fit yields $2J_z\mu_B = 5.7\pm0.9\ \mu_B/Eu^{2+}$ and $m_0 = (1.3 \pm0.5) \times 10^2\ \mu_B/nm^2$. This value for $2J_z\mu_B$ is in good agreement with the control sample of Si(111)/EuS, as well as previously reported values.[22,29] The nonzero intercept represents an induced moment in Bi_2Se_3 at the interface: a maximum estimated value ~ 20 μ_B/nm^2 based on n_{3D} and Landé g factor g ~ 50 of Bi_2Se_3.[30] This extra moment can be expected to come from the magnetized interfacial atoms as well as that due to the polarization of the electron gas in Bi_2Se_3.[31] Possible spin polarized electronic states originating from the hybridizations between EuS and Bi_2Se_3 can be respected.[3,31] In particular, it could be assisted by the large Landé g factor of surface electrons.[30] Although an extensive interfacial characterization study for a detailed understanding of the coupling mechanism leading to the induced interface magnetic moment would be necessary in the future, the electrical transport and magnetic data shown here self-consistently supports the interpretation. Growth related artifacts such as clustering of EuS or Eu atoms is ruled out (cross sectional TEM studies proves this) as it cannot provide an increase of the magnetic moment. It may be noted that we can form excellent tunnel barriers even down to 0.8nm of EuS showing standard tunneling characteristics including Josephson tunneling in other systems.[6]

The above magnetization studies indicate that the interface region of Bi_2Se_3 becomes magnetized. Thus, it creates broken time-reversal symmetry and should translate into magnetic signatures in electrical transport. To confirm this, the magnetoresistance (MR), $\Delta\rho/\rho_{H=0}$, of bilayers was studied using standard Hall bar samples with in-plane magnetic fields. Figure 3a shows such a measurement for a Bi_2Se_3/EuS (1 nm EuS) sample, where an unusual feature consisting of sharp v-shaped dips in the resistance, can be seen at 1 K, and duplicated in several other samples. These dips are hysteretic, that is, they appear once for a given direction of the field sweep. The temperature dependence of the magnitude of the MR dip is shown in Fig. 3b, decreasing as temperature increases. Also plotted here is the field value where the dip occurs, H_{min}, which shows similar decrease with increasing temperature. The values of H_{min} are consistent with the H_c values, namely, H_{min} approaches H_c ~ 18 Oe at 4.8 K. These observations point to the ferromagnetic origin of the effect. While the Curie temperature T_C of the bilayer sample is large (~ 20 K), however, the hysteretic MR is only visible below around 4 K. Furthermore, the temperature dependence suggests that the hysteretic MR does not arise from charges trapped in EuS, since their conductance contribution would be activated at elevated temperatures, and thus would instead show increasing MR for increasing temperature.

The origin of this hysteretic MR appears to be unconventional, as the resistance always goes through a minimum at H_c. This minimum coincides with the zero net magnetization of the ferromagnetic system where random magnetic domains develop. These random domains are expected to have an isotropic arrangement, consistent with the observed isotropic in-plane MR shown in Fig. 3a, which is dramatically different from the anisotropic magnetoresistance (AMR) commonly seen in ferromagnetic materials.[32,33,34] Moreover, the enhancement of the conductance of Bi_2Se_3 coinciding with the domain structures at H_c is seen in all Bi_2Se_3/EuS samples. By applying a perpendicular magnetic field, Fig. 3c demonstrates that the saturation moment $M_{P,S}$ is even larger compared to $M_{I,S}$ in Fig. 2a. Furthermore, M_P shows a steeper rise with increasing field in the Bi_2Se_3/EuS (3 nm) sample compared to the 1 nm EuS grown on Si(111) (Fig. 3c inset); even though thicker EuS thin films favor in-plane anisotropy (Fig. 3). This proves that the perpendicular anisotropy is preferred for EuS films grown on Bi_2Se_3, which is attributed to the strong spin-orbit coupling of Bi_2Se_3,[35,36] as well as likely related to the large anisotropy of the g-factor for the interface electrons seen in bulk Bi_2Se_3,[37] and which may result in a canting of the magnetic moment right at the Bi_2Se_3/EuS interface (Fig. 3d). At H_c, domain walls can form in the interface magnetic layer by the formation of randomly oriented magnetic domains (Fig. 3d). The

topological surface states at the domain wall would have low mass. The chiral conduction modes are predicted to propagate along the domain wall similar to the quantum Hall edge channels.[1,2] This could enhance the overall conduction in the sample compared to the condition with no domain walls, leading to the resistance dips shown in Fig. 3a. Similar effect is seen in impurity-doped Bi_2Te_3 by tuning the Fermi level across its surface Dirac point.[13] However, in the present work this unique property of ferromagnetic TI in heterostructured thin film bilayers is observed even without the electrostatic gating, which could be advantageous for applications. As a result of the induced canted magnetization at the interface, the hysteretic *MR(T)* could differ from the *M(T)* of the overall EuS film. Both ferromagnetism of EuS and the coupling between EuS and Bi_2Se_3 have to be strong to signify this effect. On the other hand, smaller T_C of the induced interfacial ferromagnetic layer than that of EuS film can be expected due to possible quantum fluctuations,[38] and weakening of the canted interfacial spins, coupled to adjacent in-plane parallel spins, with increasing temperature may explain the lower onset temperature for the hysteretic MR. Further control of interface quality can be expected to result in higher remnant perpendicular magnetization.

Hall effect data of the control sample (with perpendicular magnetic fields up to 4 Tesla) showed linear magnetic field dependence (Fig. 4a inset), which does not change significantly with temperature. For bilayer samples (Fig. 4a and 4b), the behavior is clearly different, with features exhibiting their ferromagnetic nature. A further consequence of the ferromagnetic conducting interface is the appearance of the anomalous Hall effect (AHE).[39] Fig. 4a shows the nonlinear contribution to the Hall voltage, $\Delta V_{yx}(H)$, which is extracted by removing the dominant linear contribution. The magnitude of the saturation voltage, ΔV_{yx}^{M}, versus temperature is shown in Fig. 4b. Here, $\Delta V_{yx}^{M}(T)$ is seen to increase steeply below T_C. The temperature at the onset of the steep rise is higher for the Bi_2Se_3/EuS (3 nm) sample than for the Bi_2Se_3/EuS (1 nm) sample, commensurate with the higher T_C for thicker EuS films.[40] In addition, $\Delta V_{yx}^{M}(T)$ and $M(T)$ have similar temperature dependence (Fig. 4c), and $V_{yx}^{M}(H)$ and $M(H)$ have similar field dependence (Fig. 4c inset), clearly pointing to the ferromagnetic origin of $\Delta V_{yx}(H)$. On the other hand, the control sample of Bi_2Se_3 capped with Al_2O_3 didn't show this sharp rise below ~ 15 K in non-linear Hall signal. The existence of AHE further confirms the induced ferromagnetic order in Bi_2Se_3. Finally, the dominance of the ordinary Hall voltage over the much smaller AHE voltage might be due to the parallel bulk conducting channel of the 20 nm Bi_2Se_3 that shorts the AHE signal.[13] By reducing the bulk carrier density one could expect a well-defined AHE, as well as a larger hysteretic MR in TI/FI heterostructures.

In summary, Bi_2Se_3/EuS heterostructures exhibit proximity-induced interfacial magnetization. This effect originates from a uniform exchange field over the TI surface, without structurally disturbing the TI. This local symmetry breaking technique not only enables the creation of cleaner ferromagnetic TI systems with larger surface exchange gaps, superior to the approach with magnetic impurity doping,[41] but also allows a greater freedom in nano-patterning lateral TI heterostructures, where designated regions with broken time-reversal symmetry can be created. Similar heterostructures have the potential of developing a variety of technologically advanced devices based on the predicted novel electrical excitations in TI. For example, devices holding zero-field quantum Hall edge channels could be fabricated using TI films sandwiched by FI; as well as systems holding Majorana bound states through the patterning of FI on superconducting TI surfaces.

Acknowledgements
The authors acknowledge the valuable discussion and assistance of P.A. Lee, L. Fu, J. Shi, S-Q. Shen, G-X. Miao and H-Z. Lu. We would like to thank support from the MIT MRSEC through the MRSEC Program of the NSF under award number DMR-0819762. Part of this work was carried out at the CMSE shared experimental facilities. P.W., B.A.A, D.H. and J.S.M. would like to thank support from NSF DMR grants 1207469 and 0907007, and ONR grant N00014-09-1-0177.

References:
1 X.-L. Qi & S.-C. Zhang. *Rev Mod Phys* **83**, 1057-1110, (2011).
2 M. Z. Hasan & C. L. Kane. *Rev Mod Phys* **82**, 3045-3067, (2010).
3 P. G. De Gennes. *Phys Lett* **23**, 10-11, (1966).

4 G. Sarma. *J Phys Chem Solids* **24**, 1029-1032, (1963).
5 X. Hao, J. S. Moodera & R. Meservey. *Phys Rev Lett* **67**, 1342-1345, (1991).
6 J. S. Moodera, T. S. Santos & T. Nagahama. *J Phys-Condens Mat* **19**, 165202, (2007).
7 X. L. Qi, T. L. Hughes & S. C. Zhang. *Phys Rev B* **78**, 195424, (2008).
8 A. M. Essin, J. E. Moore & D. Vanderbilt. *Phys Rev Lett* **102**, -, (2009).
9 X. L. Qi, R. D. Li, J. D. Zang & S. C. Zhang. *Science* **323**, 1184-1187, (2009).
10 Y. L. Chen *et al. Science* **329**, 659-662, (2010).
11 L. A. Wray *et al. Nat Phys* **7**, 32-37, (2011).
12 P. P. J. Haazen *et al. Appl Phys Lett* **100**, 082404-082403, (2012).
13 J. G. Checkelsky, J. Ye, Y. Onose, Y. Iwasa & Y. Tokura. *Nat Phys* **8**, 729-733, (2012).
14 S.-Y. Xu *et al. Nat Phys* **8**, 616-622, (2012).
15 Q. Liu, C.-X. Liu, C. Xu, X.-L. Qi & S.-C. Zhang. *Phys Rev Lett* **102**, 156603, (2009).
16 I. Vobornik *et al. Nano Lett* **11**, 4079-4082, (2011).
17 L. Fu & C. L. Kane. *Phys Rev Lett* **100**, 096407, (2008).
18 A. C. Potter & P. A. Lee. *Phys Rev B* **83**, 094525, (2011).
19 Y. S. Hor *et al. Phys Rev Lett* **104**, 057001, (2010).
20 M.-X. Wang *et al. Science* **336**, 52, (2012).
21 G.-X. Miao, M. Müller & J. S. Moodera. *Phys Rev Lett* **102**, 076601, (2009).
22 G. Miao. *Appl. Phys. Lett.* **94**, 182504, (2009).
23 I. Garate & M. Franz. *Phys Rev Lett* **104**, 146802, (2010).
24 T. Yokoyama, Y. Tanaka & N. Nagaosa. *Phys Rev B* **81**, 121401, (2010).
25 J. Chen *et al. Phys Rev Lett* **105**, 176602, (2010).
26 X. Wang *et al. Physica E: Low-dimensional Systems and Nanostructures* **46**, 236-240, (2012).
27 H. Steinberg, J. B. Laloë, V. Fatemi, J. S. Moodera & P. Jarillo-Herrero. *Phys Rev B* **84**, 233101, (2011).
28 A. Mauger & C. Godart. *Physics Reports* **141**, 51-176, (1986).
29 M. Muller, R. Schreiber & C. M. Schneider. *J Appl Phys* **109**, 07C710-713, (2011).
30 J. G. Analytis *et al. Nat Phys* **6**, 960-964, (2010).
31 See EPAPS material.
32 T. McGuire & R. Potter. *Magnetics, IEEE Transactions on* **11**, 1018-1038, (1975).
33 C. Gould *et al. Phys Rev Lett* **93**, 117203, (2004).
34 S. Y. Huang *et al. Phys Rev Lett* **109**, 107204, (2012).
35 C. Chappert & P. Bruno. *J Appl Phys* **64**, 5736-5741, (1988).
36 L. Néel. *J. Phys. Radium* **15**, 225-239, (1954).
37 H. Köhler & E. Wöchner. *physica status solidi (b)* **67**, 665-675, (1975).
38 F. S. Nogueira & I. Eremin. *Phys Rev Lett* **109**, 237203, (2012).
39 N. Nagaosa, J. Sinova, S. Onoda, A. H. MacDonald & N. P. Ong. *Rev Mod Phys* **82**, 1539-1592, (2010).
40 R. Schiller & W. Nolting. *Solid State Commun* **110**, 121-125, (1999).
41 W. Luo & X. L. Qi. *eprint arXiv:1208.4638*, (2012).

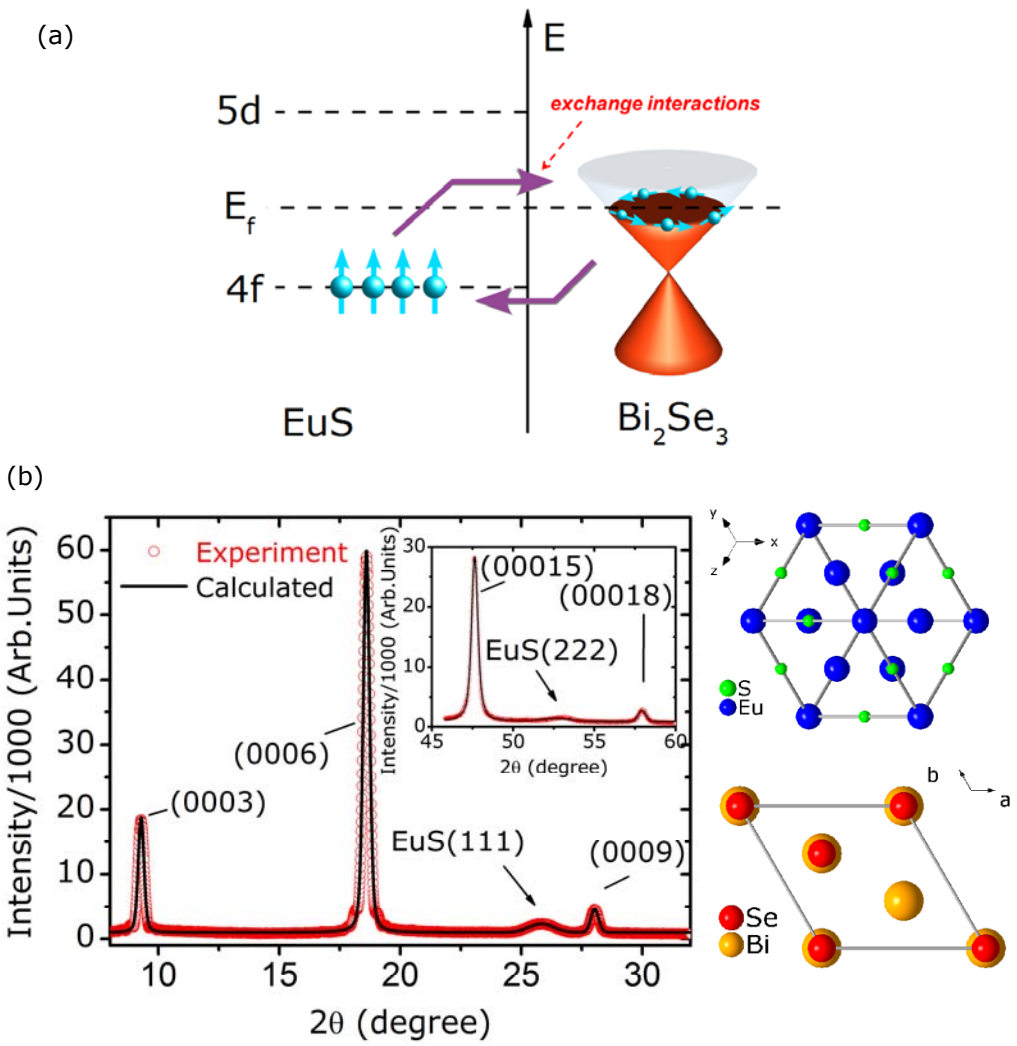

Figure 1: (a) The diagram illustrates the ferromagnetic exchange interaction between Bi_2Se_3, and EuS. (b) The measured (red) and calculated (black) out-of-plane X-ray diffraction scan for a high-quality epitaxial Bi_2Se_3[0001]//EuS[111] bilayer. The inset shows the data at larger angles. The two cartoon images show the lattice structures of EuS along the [111] direction and Bi_2Se_3 along the [0001] direction.

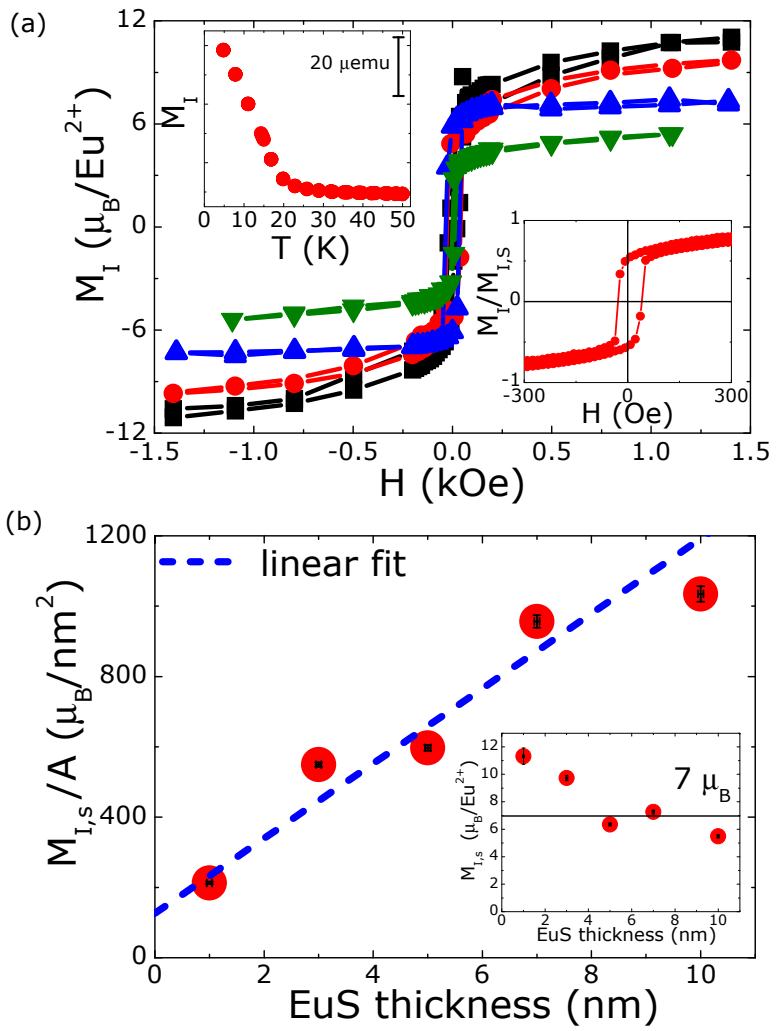

Figure 2: (a) Magnetic moment per Eu^{2+} ion as a function of magnetic field of Bi_2Se_3/EuS bilayer samples for three thicknesses of EuS: 1 nm (black squares), 3 nm (red circles) and 7 nm (blue up triangles), measured at 4.8 K. The magnetic field was applied in the film plane. The control sample data for 1 nm EuS on Si(111) is shown in green down triangles. The inset shows the temperature dependence of the magnetic moment, and the low-field hysteresis for the Bi_2Se_3/EuS (3 nm) sample. (b) Saturation magnetic moment per unit area (see text) as a function of the thickness of the EuS layers, where the nonzero intercept is the induced interfacial magnetic moment. The size of the data points includes the error in *M* and film thickness. The inset shows the saturation magnetic moment (at 1.5 kOe) per Eu^{2+} ion as a function of EuS thickness.

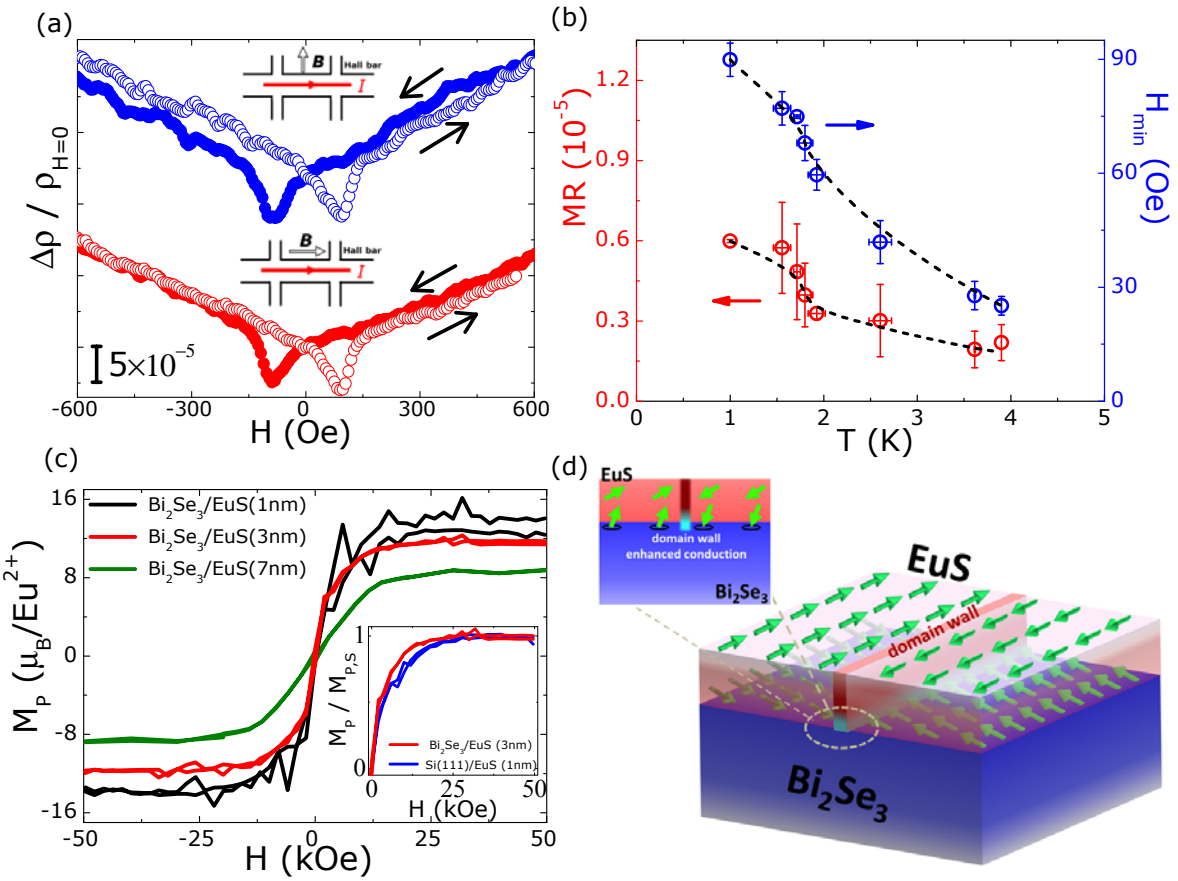

Figure 3: (a) Planar magnetoresistivity as a function of applied in-plane magnetic field of a Bi_2Se_3/EuS (1 nm) sample at T = 1.0 K showing hysteretic minima at the coercive field positions. Curves are shifted for clarity. The inset shows the corresponding field and current directions in the Hall bar. (b) MR ratio (magnitude of MR dip) and the coercive field H_C as a function of temperature. (c) Perpendicular magnetic moment per Eu^{2+} ion, M_P, at large fields. Inset shows the faster saturation of M_P for the Bi_2Se_3/EuS (3 nm) sample compared to 1 nm EuS grown on Si(111). (d) Schematic diagram showing the inferred magnetic moment distribution in magnetic domains of Bi_2Se_3/EuS interface. A perpendicular domain wall (denoted in light blue) may form at the interface that enhances the overall sample conduction.

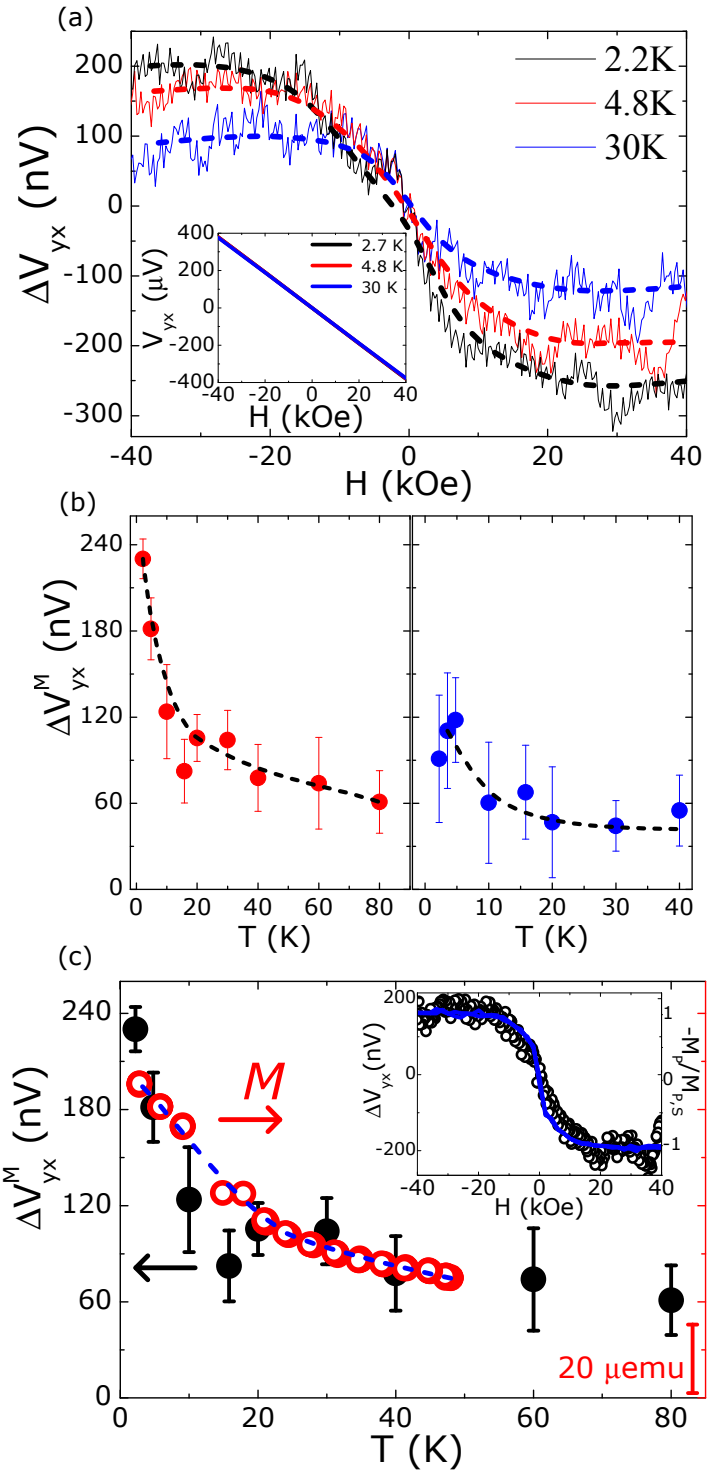

Figure 4: (a) Nonlinear contribution to the Hall voltage, $\Delta V_{yx}(H)$, as a function of applied perpendicular magnetic field at three temperatures. Inset shows Hall voltage $V_{yx}(H)$ of the control sample Bi_2Se_3. (b) Saturated nonlinear Hall voltage, ΔV_{yx}^{M}, as a function of temperature for Bi_2Se_3/EuS (1 nm) (right) and Bi_2Se_3/EuS (3 nm) (left). (c) Comparison of $\Delta V_{yx}^{M}(T)$ (black solid dots) to the magnetization $M(T)$ (red open circles) for the Bi_2Se_3/EuS (3 nm) sample. The inset compares $\Delta V_{yx}(H)$ (open circles) to $M(H)$ (solid line), illustrating the saturation occurring at high perpendicular fields.